International Journal of Nanomedicine

Dovepress
open access to scientific and medical research

Open Access Full Text Article

ORIGINAL RESEARCH

Ultrasound molecular imaging of breast cancer in MCF-7 orthotopic mice using gold nanoshelled poly(lactic-co-glycolic acid) nanocapsules: a novel dual-targeted ultrasound contrast agent

This article was published in the following Dove Press journal:
International Journal of Nanomedicine

Li Xu[1,*]
Jing Du[1,*]
Caifeng Wan[1]
Yu Zhang[1]
Shaowei Xie[1]
Hongli Li[1]
Hong Yang[2]
Fenghua Li[1]

[1]Department of Ultrasound, Renji Hospital, School of Medicine, Shanghai Jiao Tong University, Shanghai, China; [2]Department of Chemistry, College of Life and Environmental Science, Shanghai Normal University, Shanghai, China

*These authors contributed equally to this work

Background: The development of nanoscale molecularly targeted ultrasound contrast agents (UCAs) with high affinity and specificity is critical for ultrasound molecular imaging in the early detection of breast cancer.

Purpose: To prospectively evaluate ultrasound molecular imaging with dual-targeted gold nanoshelled poly(lactide-co-glycolic acid) nanocapsules carrying vascular endothelial growth factor receptor type 2 (VEGFR2) and p53 antibodies (DNCs) in MCF-7 orthotopic mice model.

Methods: DNCs were fabricated with an inner PLGA and outer gold nanoshell spherical structure. Its targeting capabilities were evaluated by confocal laser scanning microscopy (CLSM) and flow cytometry (FCM) in vitro. Contrast-enhanced ultrasound imaging (CEUS) with DNCs was evaluated qualitatively and quantitatively in vitro and in MCF-7 orthotopic mice model by two different systems. The biodistribution of NCs in mice was preliminary investigated. Differences were calculated by using analysis of variance.

Results: DNCs showed a well-defined spherical morphology with an average diameter of 276.90±110.50 nm. In vitro, DNCs exhibited high target specificities (79.01±5.63% vs. 2.11±1.07%, $P<0.01$; 75.54±6.58% vs. 5.21±3.12%, $P<0.01$) in VEGFR2- and p53-positive cells compared with control cells. In vivo, CEUS displayed a significantly higher video intensity in two systems using DNCs in comparison with non-targeted PLGA@Au NCs and single-targeted NCs. Biodistribution studies revealed that more DNCs in breast cancer tissue could be detected in mice than in other NCs ($P<0.05$).

Conclusion: DNCs were demonstrated to be novel dual-targeted UCAs and may have potential applications in early non-invasive visualization of breast cancer.

Keywords: ultrasound molecular imaging, targeted ultrasound contrast agent, poly(lactic-co-glycolic acid); antibody, breast cancer

Correspondence: Fenghua Li
Department of Ultrasound, Renji Hospital, School of Medicine, Shanghai Jiao Tong University, 160 Pujian Road, Shanghai 200127, China
Tel/fax +86 21 6838 3371
Email fenghua-li@163.com

Hong Yang
Department of Chemistry, College of Life and Environmental Science, Shanghai Normal University, 100 Guilin Road, Shanghai 200234, China
Tel/fax +86 21 6432 8981
Email yanghong@shnu.edu.cn

Introduction

Breast cancer is the leading cause of cancer-related death in women. Earlier detection of breast cancer can reduce death from the disease substantially.[1] Digital mammography is the most frequently undertaken imaging procedure for breast cancer screening. Magnetic resonance imaging and ultrasound (US) have important roles in the diagnosis, staging, and follow-up of breast cancer.[2]

Unlike conventional imaging which, in general, detects the anatomic or phenotypic changes that occur as the end result of a biologic process, molecular imaging helps to identify more subtle changes non-invasively, even at cellular or molecular

submit your manuscript | www.dovepress.com
Dovepress
http://dx.doi.org/10.2147/IJN.S153993

© 2018 Xu et al. This work is published and licensed by Dove Medical Press Limited. The full terms of this license are available at https://www.dovepress.com/terms.php and incorporate the Creative Commons Attribution – Non Commercial (unported, v3.0) License (http://creativecommons.org/licenses/by-nc/3.0/). By accessing the work you hereby accept the Terms. Non-commercial uses of the work are permitted without any further permission from Dove Medical Press Limited, provided the work is properly attributed. For permission for commercial use of this work, please see paragraphs 4.2 and 5 of our Terms (https://www.dovepress.com/terms.php).

levels, before detectable changes in the phenotype have developed.[3–6] For early detection of breast cancer, in which repetitive imaging examinations are warranted (eg, dense breast tissue for which mammography has limited accuracy for detecting breast cancer), ultrasound molecular imaging (USMI) is advantageous because it can detect small foci of cancer with high sensitivity and specificity without the use of potentially harmful ionizing radiation. Also, USMI is less expensive compared with other imaging methods.[7]

The key component involved in the USMI of breast cancer is the development of suitable probes such as targeted ultrasound contrast agents (tUCAs), which can reach the cancerous lesion specifically in vivo.[2] Solid tumors exhibit the enhanced permeability and retention effect due to the "leaky" vasculature and inadequate lymphatic drainage system they possess.[8,9] Nanoscale tUCAs could access the extravascular space whereas microscale tUCAs are restricted to the vascular compartment.[10]

Recent advancements in nanomaterial preparation have elicited significant impacts for the potential clinical diagnosis of breast cancer. The biocompatible and biodegradable polymer poly(lactic-co-glycolic acid) (PLGA) has been approved by the Food and Drug Administration of USA for drug-delivery systems and shows contrast-enhancing capability in US.[11,12] Gold (Au) nanostructures display good biocompatibility as well as excellent optical properties, thus allowing their use in biologic and medical applications.[13] It has been reported that the combination of Au nanoshells and PLGA as a "shell-core structure" could be used in US.[14,15] Au nanoshells on the outer surface could enhance the reflection of the agents, and act as photoabsorbers in near-infrared photothermal therapy. Ke et al prepared a series of theranostic agents based on Au nanoshells and poly(lactic acid) microcapsules to realize modal US and other contrast-imaging diagnoses.[16,17] Xi et al developed Au nanoparticle (NP)-coated, polydopamine-modified, PLGA hybrid capsules for combined US imaging and high-intensity focused US therapy.[18] However, those agents could not identify target sites from molecular levels or combine with molecules with high specificity for an appropriately long time because high affinity-binding ligands on the surface of the agents were absent. Furthermore, few studies have been conducted to develop targeted Au-nanoshelled PLGA NPs for the early diagnosis of breast cancer or to investigate the biodistribution of Au-nanoshelled PLGA NPs in vivo.

Owing to its heterogeneity, breast cancer is one of the most challenging solid tumors to diagnose and treat.[19] Optimal targets should be identified to develop breast cancer-specific USMI probes. Vascular endothelial growth factor receptor type 2 (VEGFR2) is a transmembrane receptor tyrosine kinase. It is a well-studied molecular marker that is overexpressed on cancerous angiogenic vascular endothelial cells.[20–23] Several studies have demonstrated that targeting VEGFR2 allows breast cancer detection using USMI.[7,24–26] The 53-kD nuclear phosphoprotein p53 has been implicated in the control of cell-cycle regulation, cell differentiation, and the surveillance of genomic integrity. Disruption of the p53 pathway is one of the most common genetic alterations in several tumor types, including those of the breast.[27,28] Milicevic et al reported that expression of p53 protein may be an early event in breast cancer progression.[29] Our research team has designed and assessed p53-targeted PLGA@Au nanocapsules (NCs). Our results suggest that NCs have good targeting capability and US contrast enhancement in vitro.[30]

In the present study, our basic idea was to upgrade single-targeted PLGA@Au NCs to dual-targeted PLGA@Au NCs for specific USMI of breast cancer and investigate the biodistribution of targeted PLGA@Au NCs in vivo. Dual-targeted gold nanoshelled poly(lactic-co-glycolic acid) nanocapsules carrying anti-vascular endothelial growth factor receptor type 2 antibody and anti-p53 antibody (DNCs) were synthesized by filling perfluoropropane (C_3F_8) into PLGA NCs, followed by the formation of Au nanoshells on the surface, and then conjugation with anti-VEGFR2 and anti-p53 antibodies (Scheme 1). We expected sufficient accumulation of agents in tumor regions to be achieved by targeting the tumor vasculature and tumor cells of nanoscale size. PLGA NCs provide the hollow core that could be a basis for US-responsive properties, and Au nanoshells on the outer surface could enhance the reflection of agents and display NC biodistribution in vivo. Such a dual-targeted agent could offer high diagnostic accuracy and reliability using USMI in MCF-7 orthotopic mice (Scheme 1).

Materials and methods

Materials

PLGA (carboxylic acid terminated, lactide:glycolide 50:50, molecular weight (Mw) 24,000–38,000) and poly(allylamine hydrochloride; PAH, Mw~17,500) were supplied by Sigma-Aldrich Trading Co., Ltd (Shanghai, China). Tetrachloroauric (III) acid trihydrate ($HAuCl_4 \cdot 3H_2O$) was purchased from Acros Organics (Morris, NJ, USA). Thiol, Carboxyl-terminated poly (ethylene glycol; SH-PEG-COOH, Mw 2000) was supplied by Xi'an Ruixi Biological Technology Co., Ltd (Xi'an, China). Hydroxylamine hydrochloride 1-(3-Dimethylaminopropyl)-3-ethylcarbodiimide hydrochloride (EDC) and N-Hydroxysuccinimide (NHS) were purchased from Aladdin Chemistry Co., Ltd (Shanghai, China).

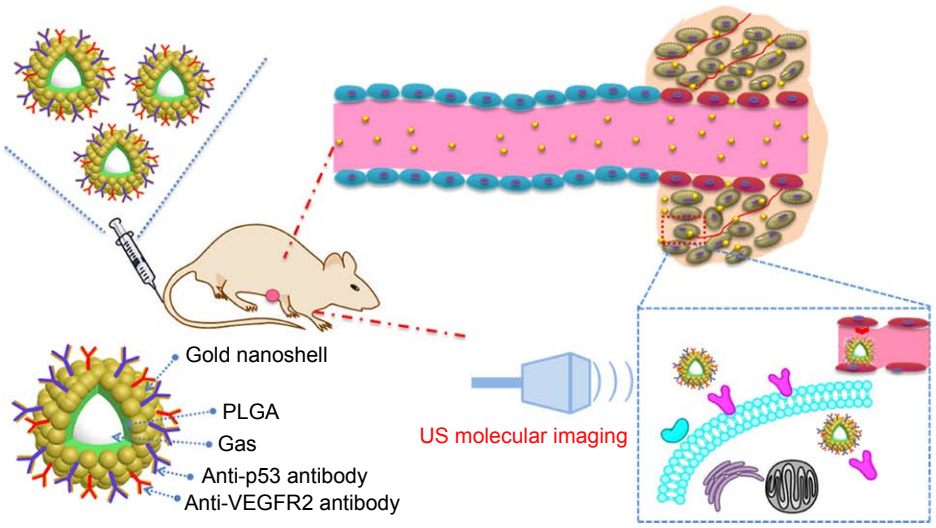

Scheme 1 Schematic illustration of the structure of DNCs and the ultrasound molecular imaging process using the dual targeted agent.
Note: DNCs, dual-targeted gold nanoshelled poly(lactic-co-glycolic acid) nanocapsules carrying anti-vascular endothelial growth factor receptor type 2 antibody and anti-p53 antibody.
Abbreviations: PLGA, poly(lactic-co-glycolic acid); US, ultrasound; VEGFR2, vascular endothelial growth factor receptor type 2.

Fluorescein isothiocyanate (FITC)-labeled anti p53 antibody was obtained from Abcam (Cambridge, MA, USA). Phycoerythrin (PE)-conjugated anti VEGFR2 antibody and Matrigel were purchased from Becton, Dickinson Clontech (Palo Alto, CA, USA). 17β-Estradiol (0.72 mg/60 days) was supplied by Innovative Research (Sarasota, FL, USA). All other reagents without further instruction were used as received.

Preparation of PLGA@Au NCs

PLGA@Au NCs were prepared according to methods described previously.[15,16,30,31] Briefly, PLGA NCs were synthesized using an adapted oil-in-water emulsion solvent-evaporation process. PLGA (100 mg) and camphor (10 mg) were dissolved in 3.5 mL methylene chloride (oil phase). Then, an oil-in-water emulsion was generated by adding the oil phase dropwise to an aqueous solution of polyvinyl alcohol (2% w/v, 20 mL; water phase). The system was emulsified using an ultrasonic probe in an ice bath and sonicated for 120 s. Afterwards, the emulsion was stirred for 5 h and centrifuged and washed with deionized water. Finally, the NCs were freeze-dried and filled with C_3F_8 gas. Then, PLGA NCs were added to PAH solution (10 mL, 1.0 mg/mL in 0.5 M NaCl aqueous solution) and stirred for 30 min, then centrifuged and washed. Meanwhile, a citrate-stabilized solution containing Au NPs of diameter ~6 nm was prepared via a redox reaction. $HAuCl_4$ aqueous solution (1 mL, 1% w/v) and sodium citrate solution (1.0 mL, 1% w/v) were added to deionized water (98 mL) with vigorous stirring for 5 min. Then, $NaBH_4$ (1.0 mL, 0.075% w/v) in sodium citrate (1% w/v) solution was added and stirred continuously for 15 min to form Au NPs. The precipitate of PLGA/PAH NCs was suspended into citrate-stabilized Au NPs solution and the centrifuge/wash step repeated to obtain Au NPs-coated PLGA NCs via surface seeding. Afterwards, the Au NPs-coated PLGA NCs were re-dispersed and added to $HAuCl_4$ (2 mL, 1% w/v) solution with stirring. Then, $NH_2OH{\cdot}HCl$ solution (0.3 mL, 0.5 mol/L) was added to reduce $HAuCl_4$, which enabled the formation of Au nanoshells around the surface of PLGA NCs.

Preparation of targeted PLGA@Au NCs

SH-PEG-COOH (5 mg) was added to 1 mL of (1 mg/mL) PLGA@Au NCs aqueous solution, mixed thoroughly, stirred for 12 h at room temperature, and then centrifuged and washed. The precipitate was re-dispersed into 2 mL of PBS and then 10 mg each of NHS and EDC was introduced to activate the carboxylic acid groups on the surface of PLGA@Au-SH-PEG-COOH NCs. The mixture was stirred gently for 1 h at room temperature, and then the centrifuge/wash step was repeated to obtain activated PLGA@Au NCs. The solution was re-dispersed into 1.2 mL of PBS and divided into 4 equal parts. These were used as follows. Single-targeted gold nanoshelled poly(lactic-co-glycolic acid) nanocapsules carrying anti-vascular endothelial growth factor receptor type 2 antibody (VNCs) were prepared using 20 μg of single-targeted gold nanoshelled poly(lactic-co-glycolic acid) nanocapsules carrying anti-p53 antibody (PNCs) were prepared using 20 μg of anti-p53 antibodies labeled with FITC. DNCs were prepared using an equal amount of appropriate antibodies. For the control group, 20 μL of PBS was added to 1 part of solution. All these preparations were incubated in a thermostatic oscillator for 60 min. Then, pure targeted PLGA@Au NCs were obtained by removing the free antibodies.

Characterization

Scanning electron microscopy (SEM) images were obtained with a S-4800 field emission scanning electron microscope (Hitachi, Tokyo, Japan). A high-resolution transmission electron microscope (JEM-2100; JEOL, Tokyo, Japan) was used to obtain transmission electron microscopy (TEM) images to observe the morphology and structure of NCs. The size, polydispersity index (PI) and zeta potential of NCs were measured using a dynamic laser scattering (DLS) instrument (Zetasizer Nano ZS3690; Malvern Instruments, Malvern, UK). The concentration of Au element in targeted PLGA@Au NCs was determined by inductively coupled plasma-atomic emission spectroscopy (ICP-AES) using a Vista MPX ICP system (Varian Medical Systems, Palo Alto, CA, USA). The conjugation of antibodies with NCs and NCs with cells were evaluated and imaged using a confocal laser scanning microscope (TCS SP5 II; Leica, Wetzlar, Germany).

Biocompatibility

Cell culture

Human umbilical vein endothelial cells (HUVECs) overexpressing VEGFR2, mice 4T1 breast cancer cells with low expression of VEGFR2, human breast adenocarcinoma MCF-7 cells overexpressing p53 protein, and MDA-MB-231 breast cancer cells with low expression of p53 protein were provided by the Institute of Biochemistry and Cell Biology, Shanghai Institutes for Biological Sciences, Chinese Academy of Sciences (Shanghai, China). They were cultured in Dulbecco's Modified Eagle's Medium (DMEM) (Gibco, Billings, MT, USA) supplemented with 10% fetal bovine serum and 1% penicillin–streptomycin in an atmosphere of 5% CO_2 at 37°C.

DNCs cytotoxicity in vitro

In vitro cytotoxicity was determined using the 3-(4,5-dimethylthiazol-2-yl)-2,5-diphenyltetrazolium bromide (MTT) assay (Solarbio, Beijing, China) on HUVECs and MCF-7 cells. Briefly, cells (1×10^4 per well) in 100 μL of medium were seeded in a 96-well cell culture plate and cultured for 24 h. Then, the cells were exposed to serial concentrations (0, 10, 20, 50, 100, and 200 μg/mL) of DNCs and incubated further for 12 or 24 h. After removing the medium, 100 μL of MTT (0.5 mg/mL) was added to the culture and incubation continued for an additional 4 h at 37°C. Then, the culture medium was replaced with 150 μL of dimethyl sulfoxide and the absorbance was measured at 490 nm. Cytotoxicity was expressed as the percentage of viable cells compared with the percentage of untreated control cells.

DNCs' toxicity in vivo

Animal care and handling procedures were in accordance with guidelines set by the China Council on Animal Care and the protocol was revised and accepted by the ethics committee of Shanghai Slac Laboratory Animal Centre (SLAC) (SLAC-2016121001).

Healthy female BALB/c nude mice (4–6 weeks, ~20 g) were provided by SLAC (Shanghai Laboratory Animals, Shanghai, China). V&p53-PLGA@Au NCs dispersed in saline solution at a total dose of 50 μg/g were injected into the tail vein of mice (3 mice per group). Three mice receiving an injection of only physiologic (0.9%) saline were chosen to be the control group. Samples of blood and tissues were harvested from mice 12 h, 24 h, and 5 days post-injection from different groups. For serum biochemistry assays, 3 important indicators of liver function (alanine aminotransferase [ALT], aspartate aminotransferase [AST], total bilirubin [TBIL]) and 2 important indicators of renal function (creatinine, blood urea nitrogen [BUN]) were determined. After blood collection, mice were sacrificed immediately. The heart, liver, spleen, lungs, and kidneys were removed and stained with hematoxylin and eosin (H&E) stain for histology.

Specific targeting of DNCs in vitro

Confocal laser scanning microscopy (CLSM)

HUVECs, 4T1, MCF-7, and MDA-MB-231 cells at 2×10^4 cells per culture dish were incubated for 12 h. They were divided into 5 groups: non-targeted control; cells control; single-targeted (p53 or VEGFR2); targeted competition; dual-targeted. The 4 types of cells in each of the control groups were treated with 100 μL of PLGA@Au NCs for 30 min. Cells in the dual-targeted group were treated with 100 μL of DNCs for 30 min. For the VEGFR2 single-targeted group, HUVECs and 4T1 cells were treated with 100 μL of VNCs for 30 min. In the p53 single-targeted group, MCF-7 and MDA-MB-231 cells were treated with 100 μL of PNCs. Then, cells were washed thrice with PBS, fixed with 4% paraformaldehyde for 15 min, and their nuclei stained with 4,6-diamino-2-phenyl indole (DAPI) solution. Finally, the samples were evaluated and imaged using a confocal laser scanning microscope.

Flow cytometry

The green and red emissions of FITC and PE groups in NCs serve as markers to determine the cellular affinity of the material quantitatively. The groupings and treatment of cells were consistent with CLSM. All cells were centrifuged after digestion with trypsin. The supernatants were discarded and the cells were re-suspended in 1 mL of sterile PBS and collected in test tubes at 2×10^5 cells per tube prior to flow cytometry. All experiments were repeated thrice.

US in vitro

Preliminary evaluation of the US-contrast behavior of DNCs in vitro was carried out using an ultrasonic diagnostic instrument (L90; Esaote, Genova, Italy) with a 522 transducer. DNCs, VNCs, PNCs, and PLGA@Au NCs at an identical concentration (0.5 mg/mL) were dispersed in degassed deionized water in tubes (2 mL). Pure degassed deionized water was injected into the same tube to serve as the background control. Samples were scanned using the transducer in contrast mode (mechanical index, 0.10; frequency, 3–9-MHz) in a tank filled with degassed deionized water.

US in vivo

Establishment of a breast cancer model in MCF-7 orthotopic mice

Female BALB/c nude mice (4–6 weeks, ~20 g) were injected with 200 µL of a suspension of MCF-7 cells (5×10^7) mixed with Matrigel™ (Corning, Corning, NY, USA) in the second right mammary fat pad 3 days after 17β-estradiol tablets had been embedded (subcutaneously) on the left side of the neck. Imaging experiments were conducted once the tumor volume reached 200–300 mm^3. Invasive procedures were undertaken under anesthesia.

Animals

Nude mice bearing the tumor were divided into 5 groups (3 mice per group): non-targeted control; targeted competition; p53-targeted; VEGFR2-targeted; and dual-targeted. Animals were anesthetized using chloral hydrate (4.5%, 0.1 mL/10 g), and a saline solution of NCs (5 mg/mL, 200 µL) was injected in 1 portion via the tail vein. Mice in the targeted competition group were injected with 20 µL of the corresponding antibody (diluted with physiologic saline to 200 µL) 30 min before the injection of NCs solution. All mice were observed with 2 imaging systems.

The flowchart of the process and procedures of US in vivo is shown in Scheme 2.

In vivo targeted US using a 22-MHz probe

US was carried out using an ultrasonic diagnostic instrument (MyLab™ Twice; Esaote, Genoa, Italy) with a 22-MHz linear transducer (focal length, 7 mm; mechanical index,

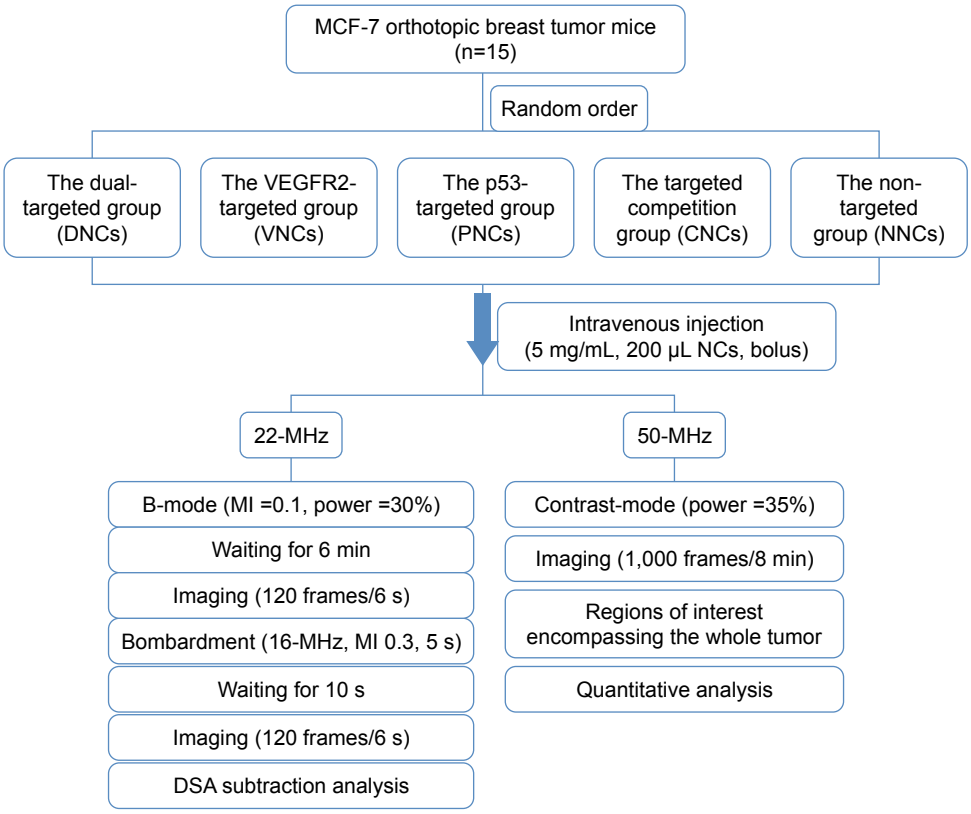

Scheme 2 Flowchart of the process and the procedures of ultrasound imaging in vivo.
Notes: CNCs, free antibodies pre-treated before DNCs application; DNCs, dual-targeted gold nanoshelled poly(lactic-co-glycolic acid) nanocapsules carrying anti-vascular endothelial growth factor receptor type 2 antibody and anti-p53 antibody; NNCs, non-targeted gold nanoshelled poly(lactic-co-glycolic acid) nanocapsules; PNCs, single-targeted gold nanoshelled poly(lactic-co-glycolic acid) nanocapsules carrying anti-p53 antibody; VNCs, single-targeted gold nanoshelled poly(lactic-co-glycolic acid) nanocapsules carrying anti-vascular endothelial growth factor receptor type 2 antibody.
Abbreviations: DSA, DigSubAna, a quantitative analytical software; MI, mechanical index; NCs, nanocapsules.

0.10; transmission power, 30%; gain, 60%). All imaging was undertaken in fundamental brightness (B) mode. US gel was used as a coupling agent on mice skin. An acoustic focus was placed at the tumor center at the level of the largest transverse cross-section and maintained throughout each experiment. Imaging was delayed for 6 min after intravenous injection of NCs in the tail vein of mice to allow targeted NCs to adhere to the tumor surface. Then, ~120 ultrasonographic frames were captured over 6 s. A continuous 16-MHz, high-power destructive pulse (mechanical index, 0.3) was applied for 5 s, which destroyed the NCs within the beam elevation. Ten seconds after destruction (to allow freely circulating NCs to replenish in tumor vessels within the beam elevation), 120 frames were acquired with the same US settings as before the pulse. In addition, the hind-limb adductor muscle of mice was scanned using the imaging protocol described previously as a quasi-tumor negative control. Images were recorded and analyzed offline using quantitative analytical software (DigSubAna; Shanghai Jiao Tong University, Shanghai, China). The difference in video intensity from subtraction of the pre- and post-destruction image frames was displayed by the software as green overlaying grayscale images.

In vivo targeted US using a 50-MHz probe

This imaging procedure was conducted using a dedicated small-animal, high-resolution imaging system (Prospect 3.0; S-Sharp, New Taipei City, Taiwan) and a 50-MHz (range, 30–50-MHz) high-frequency linear transducer with a dynamic range of 50 dB, depth of 3.7 mm, and power of 35%. Animals were kept on a heated stage to maintain their body temperature. US gel was used as a coupling agent on the tumor in mice. The acoustic focus was placed at the tumor center at the level of the largest transverse cross-section in B-mode and 1 frame image was stored. Then, the unit was turned to contrast mode and 1,000 frames were collected during 8 min. The enhanced video intensity was presented as green overlays on contrast images. The grayscale intensity and time–intensity curve (TIC) were measured in regions of interest encompassing the whole tumor in the imaging plane.

Tumor immunohistochemistry

After US, the animals were euthanized and tumors harvested. Some of the frozen tissue slices were fixed and strained (H&E). The other frozen tissue slices were fixed, rinsed, blocked, and then incubated with rat anti-mouse VEGFR2 antibody overnight at 4°C. Consecutive slices from each sample were used for PE-labeled cluster of differentiation (CD) 31 (marker of endothelial cells) staining to confirm VEGFR2 expression in tumor vessels. To identify nuclei, CD31-stained slices were counterstained with DAPI. p53 protein involved in tumor tissue slices was detected using 3,3′-diaminobenzidine staining, with brown granules, indicating expression of p53 protein.

Biodistribution of targeted NCs

The biodistribution of materials was detected according to the concentration of Au via ICP-AES. Animals were euthanized after imaging and the heart, liver, spleen, lungs, kidneys, and tumor were collected and weighed. Blood, urine, and feces were also collected and weighed. Tissues were digested with aqua regia, and subjected to measurement of Au concentration by ICP-AES and weight calculation of Au as the percentage of the total amount of injected materials (ID%/g).[32]

Statistical analyses

Results are the mean ± SD. Student's *t*-test was utilized to identify significant differences between experimental and control groups using SPSS v17.0 (IBM, Armonk, NY, USA). $P<0.05$ was considered significant.

Results and discussion

Characterization of NCs

Initially, PLGA NCs were synthesized via an oil-in-water synthetic process. SEM images (Figure 1A) revealed the spherical morphology and good dispersity of PLGA NCs, from which several cavities could be observed. TEM images clearly demonstrated the hollow interiors of the PLGA NCs formed by camphor sublimation (Figure 1B). DLS results confirmed that the average diameter of PLGA NCs was 235.80±70.40 nm. PLGA NCs were negatively charged, with a zeta potential of −24.70±5.05 mV, which could adsorb positively charged PAH for subsequent attachment of negatively charged citrate-stabilized Au NCs. Afterwards, the anchored Au NPs were used to nucleate the growth of an Au coating around PLGA/PAH NCs.

DNCs were prepared using SH-PEG-COOH as a "bridge" to connect antibodies and PLGA@Au NCs. In this process, the classical EDC/NHS method[33] was used to activate the carboxylic acid groups of PEGylated PLGA@Au NCs and facilitate the combination of amino groups with antibodies via covalent bonds to form a durable layer that serves as a targeted agent. DNCs maintained their spherical shape after deposition of Au shells but exhibited a rough surface morphology (Figure 1C), and their average diameter increased to ~276.90 nm. TEM images of DNCs (Figure 1D) illustrated that uniform Au NPs were distributed homogeneously on the rough surfaces of NCs. The low PI (0.17) by DLS indicated a narrow size distribution and high homogeneity of DNCs.

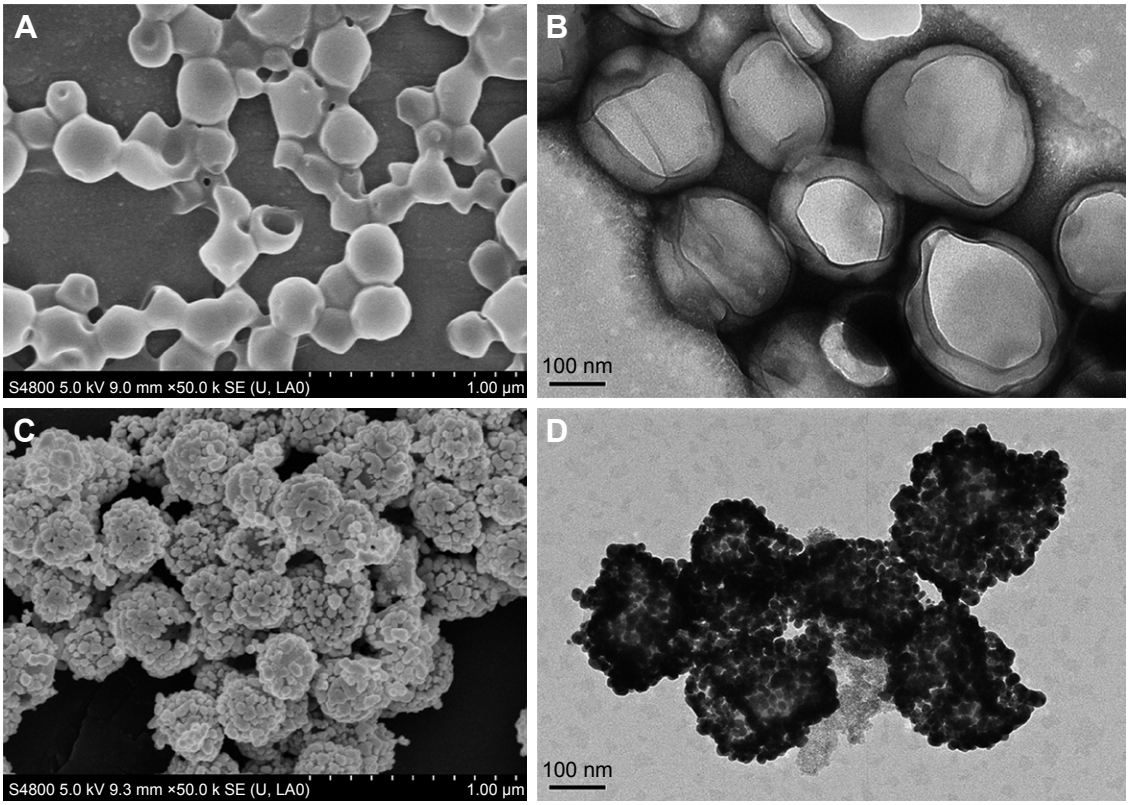

Figure 1 SEM (scale =1 μm) and TEM (scale =100 nm) of PLGA NCs (**A**, **B**) and DNCs (**C**, **D**).
Note: DNCs, dual-targeted gold nanoshelled poly(lactic-co-glycolic acid) nanocapsules carrying anti-vascular endothelial growth factor receptor type 2 antibody and anti-p53 antibody.
Abbreviations: PLGA NCs, poly(lactic-co-glycolic acid) nanocapsules; SEM, scanning electron microscope; TEM, transmission electron microscope.

The zeta potential was −24.80±4.90 mV, which implied that the solution had good stability. To investigate the stability of DNCs under physiologic conditions, DNCs were dispersed in PBS (which simulates the internal environment of body fluids). The diameters and zeta potentials of DNCs were detected at 0, 1, 2, 6, and 12 h. The size and zeta potential of DNCs changed slightly ($P>0.05$) as time elapsed (Table 1), which indicated good stability of DNCs under physiologic conditions. The amount of Au element in DNCs according to ICP-AES was 61.70% by weight.

DNCs cytotoxicity in vitro

To evaluate the biocompatibility of DNCs, MTT assays were done in vitro to investigate the toxic effects of PNCs on MCF-7 cells and HUVECs. After 24 h of incubation, >85.0% cells remained viable even at ≤200 μg/mL (Figure 2A and B). The difference in cell viabilities after 12 and 24 h of incubation was negligible, indicating the low toxicity of DNCs to these 2 cell lines. Therefore, the MTT results indicated good biocompatibility of DNCs, which could ensure safety for further US and cancer therapeutics.

DNCs toxicity in vivo

To investigate further the long-term in vivo toxicity of DNCs, healthy nude mice were injected (i.v.) with DNCs in saline solution (50 μg/g body weight). During the entire experimental period, the behaviors of all treated mice were normal, indicating negligible acute toxicity of the material. At 12 h, 24 h, and 5 days after administration, the blood and organs (heart, liver, spleen, lungs, and kidneys) were collected for serum biochemistry assays and histology, respectively, so as to quantify the potential in vivo toxicity of DNCs. Compared with the

Table 1 The stability of nanocapsules under physiological conditions ($\bar{x} \pm S$)

DNCs	0 h	1 h	2 h	6 h	12 h
Diameter (nm)	277.90±88.2	280.4±94.4	279.2±108.4	263.7±97.5	283.8±92.6
Zeta potential (mV)	−24.80±4.9	−25.6±3.8	−23.5±6.4	−24.2±7.2	−26.8±4.6

Notes: No significant statistical differences between groups ($P>0.05$). DNCs, dual-targeted gold nanoshelled poly(lactic-co-glycolic acid) nanocapsules carrying anti-vascular endothelial growth factor receptor type 2 antibody and anti-p53 antibody.

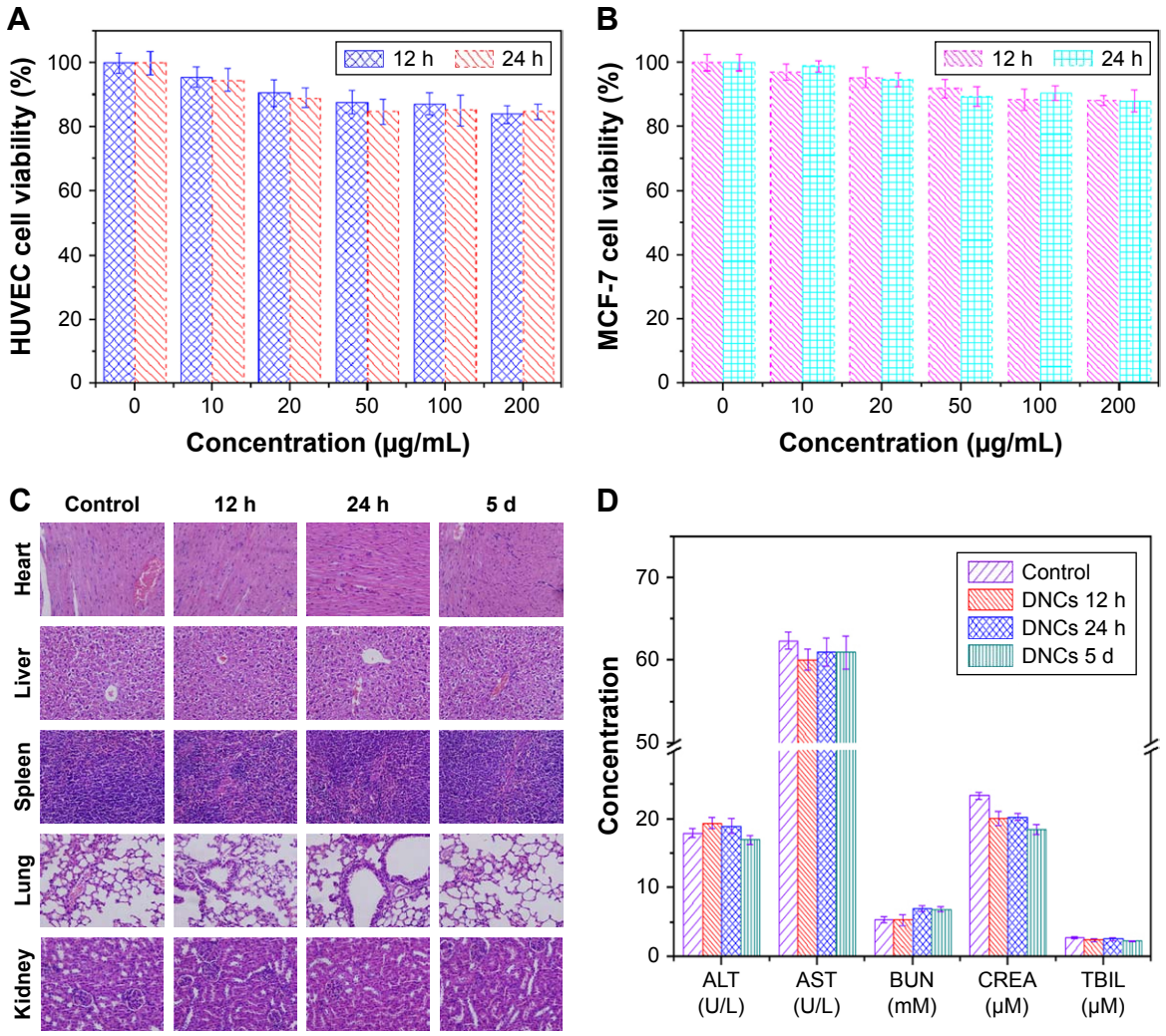

Figure 2 Cell viabilities of (**A**) HUVEC and (**B**) MCF-7 cells at different dosages of the DNCs (0, 10, 20, 50, 100, 200 μg/mL). (**C**) H&E images of heart, liver, spleen, lung, and kidney at 12 h, 24 h, and 5 days after intravenous injection of DNCs (magnification: ×100). (**D**) Serum biochemistry data for mice injected with saline solution and with DNCs (12 h, 24 h, and 5 days post-injection).

Notes: DNCs, dual-targeted gold nanoshelled poly(lactic-co-glycolic acid) nanocapsules carrying anti-vascular endothelial growth factor receptor type 2 antibody and anti-p53 antibody. Concentration units of measure in (D) were (U/L, mM, μM).

Abbreviations: ALT, alanine aminotransferase; AST, aspartate aminotransferase; BUN, blood urea nitrogen; CREA, creatinine; HUVEC, human umbilical vein endothelial cells; H&E, hematoxylin and eosin; TBIL, total bilirubin.

control group, the organs in the exposure groups maintained a similar morphology (Figure 2C), indicating that DNC administration did not cause organ damage. Serum biochemistry tests were also carried out for quantitative evaluation of 3 important indicators of liver function (ALT, AST, and TBIL) and 2 important indicators of kidney function (BUN and creatinine). These indicators were at similar levels for mice exposed to DNCs and for control mice ($P>0.05$; Figure 2D), suggesting that DNCs had good biocompatibility.

Detection of specific targeting of DNCs in vitro

CLSM PE (which shows red fluorescence) and FITC (green fluorescence) are used widely as fluorescence probes for antibody detection. Unlike previous reports,[34,35] we chose antibody-labeled fluorescence markers (VEGFR2 antibody-labeled PE and p53 antibody-labeled FITC). Thus, the connection between NCs and antibodies could be observed simply and visually by CLSM. To detect antibodies on targeted PLGA@Au NCs, NCs were loaded on a dish (Φ=20 mm) and analyzed by CLSM. As shown in Figure 3, DNCs (A), VNCs (B), PNCs (C), and NNCs (D) could be observed in bright field. Green and red signals were emitted from PE-labeled VEGFR2 antibodies and FITC-labeled p53 antibodies, respectively. VNCs displayed only red fluorescence (Figure 3B) and PNCs showed only green fluorescence (Figure 3C). Dual-targeted DNCs exhibited green and red fluorescence, indicating the presence of p53 antibodies and VEGFR2

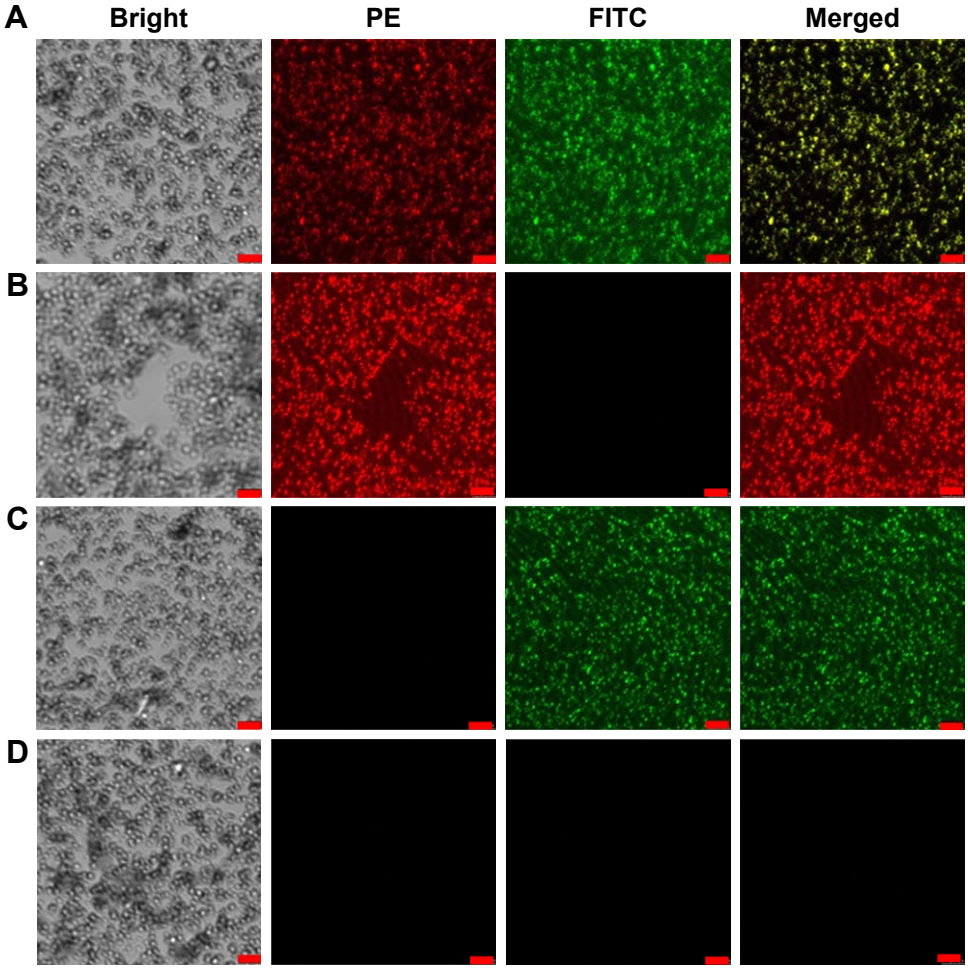

Figure 3 Confocal microscopic images of (**A**) DNCs, (**B**) VNCs, (**C**) PNCs, and (**D**) NNCs in bright field, FITC, PE, and merged channels (scale =2.5 μm), and the merged yellow signals indicate the presence of VEGFR2 and p53 in DNCs.

Notes: DNCs, dual-targeted gold nanoshelled poly(lactic-co-glycolic acid) nanocapsules carrying anti-vascular endothelial growth factor receptor type 2 antibody and anti-p53 antibody; NNCs, non-targeted gold nanoshelled poly(lactic-co-glycolic acid) nanocapsules; PNCs, single-targeted gold nanoshelled poly(lactic-co-glycolic acid) nanocapsules carrying anti-p53 antibody; VNCs, single-targeted gold nanoshelled poly(lactic-co-glycolic acid) nanocapsules carrying anti-vascular endothelial growth factor receptor type 2 antibody.

Abbreviations: FITC, fluorescein isothiocyanate; PE, phycoerythrin;

antibodies on the surface of NCs (Figure 3A). Taken together, the CLSM results provided evidence that VEGFR2 and p53 antibodies were immobilized on dual-targeted NCs.

CLSM was utilized to confirm the targeted capability of DNCs in vitro qualitatively. To demonstrate the combination of NCs and cells clearly, we show the images of the bright field (a1–f1), DAPI channel (a2–f2), PE channel (a3–f3), FITC channel (a4–f4), and merged channel (a5–f5) in Figure 4. HUVECs (A) and MCF-7 cells (C) incubated with DNCs showed green and red fluorescence, respectively, and yellow signals from merged images indicated that DNCs carrying p53 and VEGFR2 antibodies combined with positive cells. Negligible fluorescence was observed in 4T1 and MDA-MB-231 cells under similar conditions as a dual-targeted group, suggesting that DNCs could bind efficiently to cells overexpressing VEGFR2 or p53 protein. To support the receptor-mediated uptake of the DNCs, we also conducted competition experiments under the same experimental conditions by pretreating HUVEC or MCF-7 cells with free VEGFR2 or p53 antibody before the incubation of the cells with DNCs. As a result, the HUVEC (E) or MCF-7 (F) pre-treated with free antibody no longer showed distinctly higher uptake degree. The free antibody can block the binding sites of cells, resulting in the depression of the targeting capability of DNCs.

Flow cytometry

The targeting rate of DNCs was assessed further quantitatively using flow cytometry. Figure 5A was the flow cytometry results of 4T1 incubated with DNCs. HUVEC cells incubated with VNCs and DNCs were shown in Figure 5B and C. Figure 5D showed the results of

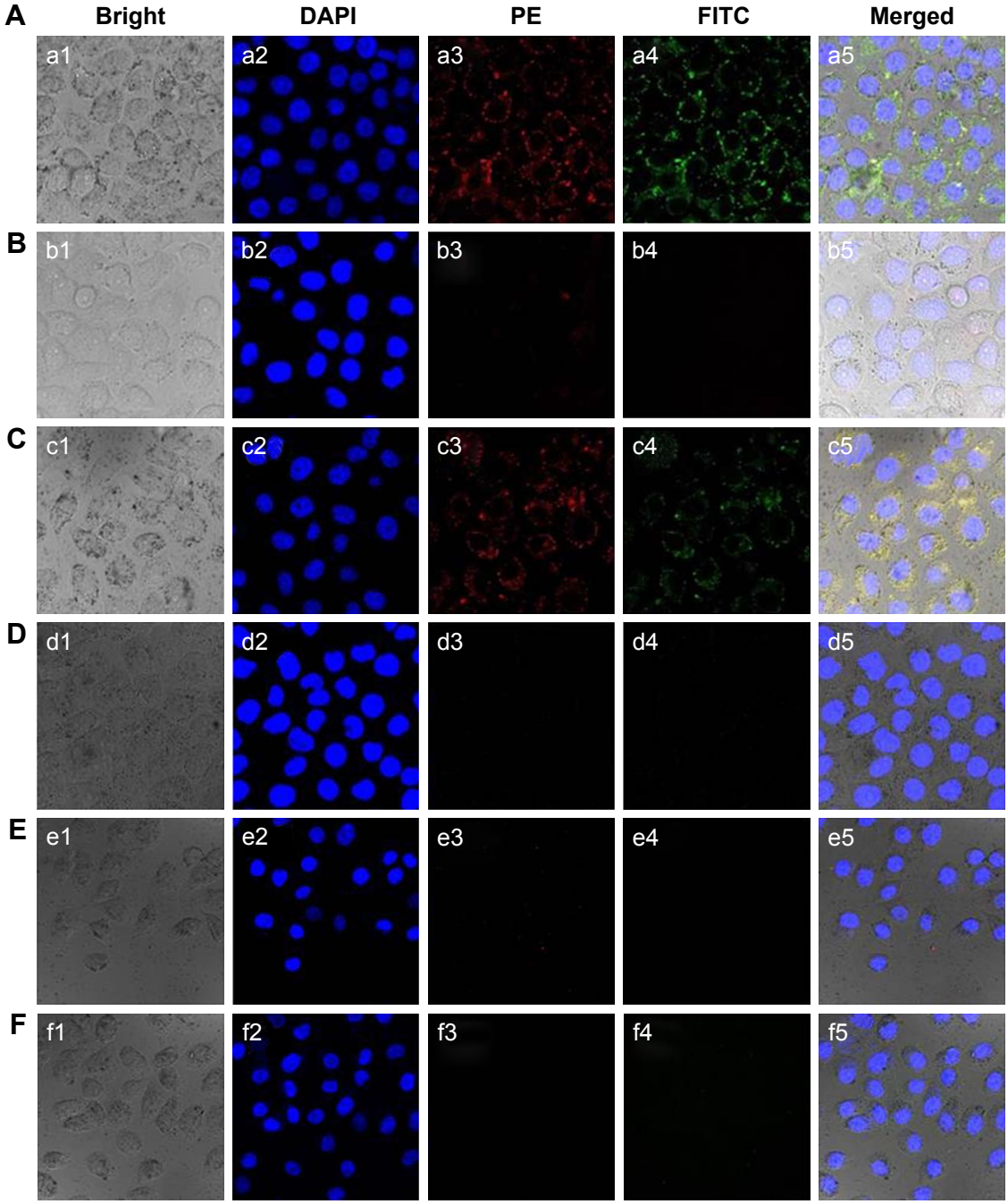

Figure 4 Confocal microscopic images of (**A**) HUVEC, (**B**) 4T1, (**C**) MCF-7, and (**D**) MDA-MB-231cells incubated with DNCs, (**E**) free VEGFR2-treated HUVEC cells incubated with DNCs and (**F**) free p53-treated HUVEC cells incubated with DNCs.

Notes: DNCs, dual-targeted gold nanoshelled poly(lactic-co-glycolic acid) nanocapsules carrying anti-vascular endothelial growth factor receptor type 2 antibody and anti-p53 antibody. a1-fi: the images of bright field; a2–f2: the images of DAPI channel; a3–f3: the images of PE channel; a4–f4: the images of FITC channel; a5–f5: the images of merged channel.

Abbreviations: DAPI, 4,6-diamino-2-phenyl indole; FITC, fluorescein isothiocyanate; HUVEC, human umbilical vein endothelial cells; PE, phycoerythrin; VEGFR2, vascular endothelial growth factor receptor type 2.

MDA-MB-231 incubated with DNCs. MCF-7 cells incubated with PNCs and DNCs were shown in Figure 5E and F. HUVECs and MCF-7 cells incubated with DNCs showed a remarkably higher targeting rate than 4T1 and MDA-MB-231 cells incubated with the same NCs (79.01%±5.63% vs 2.11%±1.07%, $P<0.01$; 75.54%±6.58% vs 5.21%±3.12%, $P<0.01$), revealing the specific targeting capability of DNCs. In addition, flow cytometry suggested no significant difference between single-targeted and dual-targeted groups in vitro ($P>0.05$), which could be ascribed to only 1 targeted protein expression in HUVECs or MCF-7 cells. Based on these results, CLSM images and

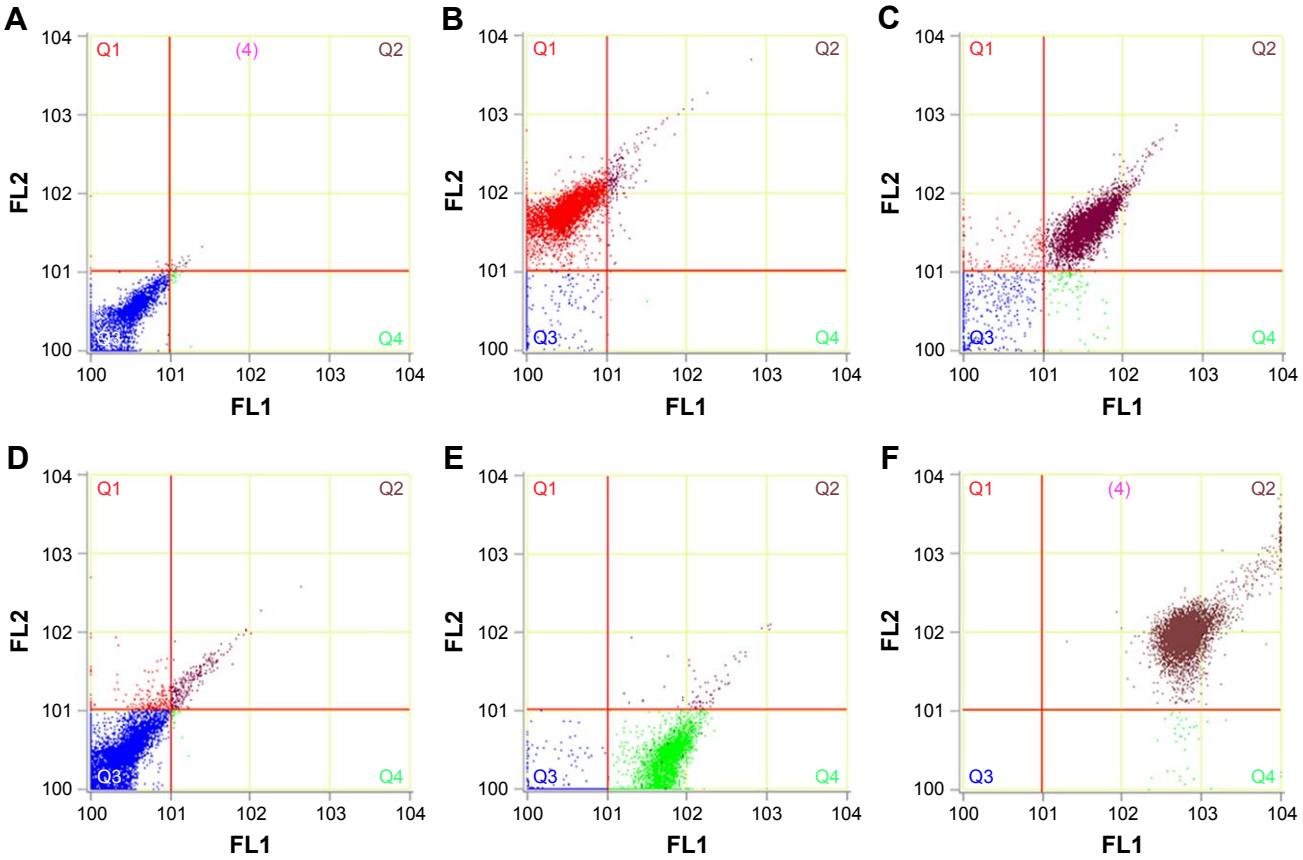

Figure 5 (**A**) The flow cytometry results of 4T1 incubated with DNCs. HUVEC cells incubated with VNCs and DNCs were shown in (**B** and **C**). (**D**) showed the results of MDA-MB-231 incubated with DNCs. MCF-7 cells incubated with PNCs and DNCs were shown in (**E** and **F**).

Notes: FLl channel showed FITC signal and FL2 channel showed PE signal. DNCs, dual-targeted gold nanoshelled poly(lactic-co-glycolic acid) nanocapsules carrying anti-vascular endothelial growth factor receptor type 2 antibody and anti-p53 antibody; PNCs, single-targeted gold nanoshelled poly(lactic-co-glycolic acid) nanocapsules carrying anti-p53 antibody; VNCs, single-targeted gold nanoshelled poly(lactic-co-glycolic acid) nanocapsules carrying anti-vascular endothelial growth factor receptor type 2 antibody.

Abbreviations: FITC, fluorescein isothiocyanate; HUVEC, human umbilical vein endothelial cells.

flow-cytometry results provided strong evidence that DNCs can recognize and combine with positive cells.

US in vitro

The ability of DNCs to be US contrast agents was assessed in vitro using a 522 transducer in contrast mode. From the contrast-enhanced ultrasound (CEUS) images shown in Figure 6, the tubes filled with DNCs (A), VNCs (B), PNCs (C), and PLGA@Au NCs (D) displayed strong dotted echoes in B-mode and CEUS images, whereas the tube filled with degassed deionized water (E) was observed as an echo. Moreover, comparative analyses using QontraXt v3.06 (Bracco, Milan, Italy) provided quantitative information via TICs. From the TIC as shown in Figure 6 (third column; in dB), DNCs showed no significant difference with single or non-targeted PLGA@Au NCs in vitro (50.40±1.86 vs 47.50±2.60, $P>0.05$; 50.40±1.82 vs 49.10±3.20, $P>0.05$; 50.40±1.83 vs 45.10±2.33, $P>0.05$), indicating that the backscattering of the NCs generated from the core-shell structure and antibodies did not weaken the effect.

Establishment of a breast cancer model in MCF-7 orthotopic mice

To better simulate the growth microenvironment of breast cancer cells, MCF-7 cells were injected into the mammary fat pads of female nude mice. A local mass appeared under the second mammary nipple of mice (Figure 7A), and a circular transplanted tumor (247±12 mm^3, n=20) with many vessels on its surface could be observed clearly after anatomization. The tumor tissue was subject to histology using H&E staining. The pathologic image of the tumor (Figure 7B) indicated that the orthotopic tumor tissues from mice were ductal carcinoma in situ. Therefore, a breast cancer model had been created in MCF-7 orthotopic mice.

US in vivo

Two systems were adopted to investigate the US-targeted contrast-enhanced capability of DNCs in the breast cancer model created in MCF-7 orthotopic mice. Imaging experiments in vivo using a 22-MHz linear transducer collected

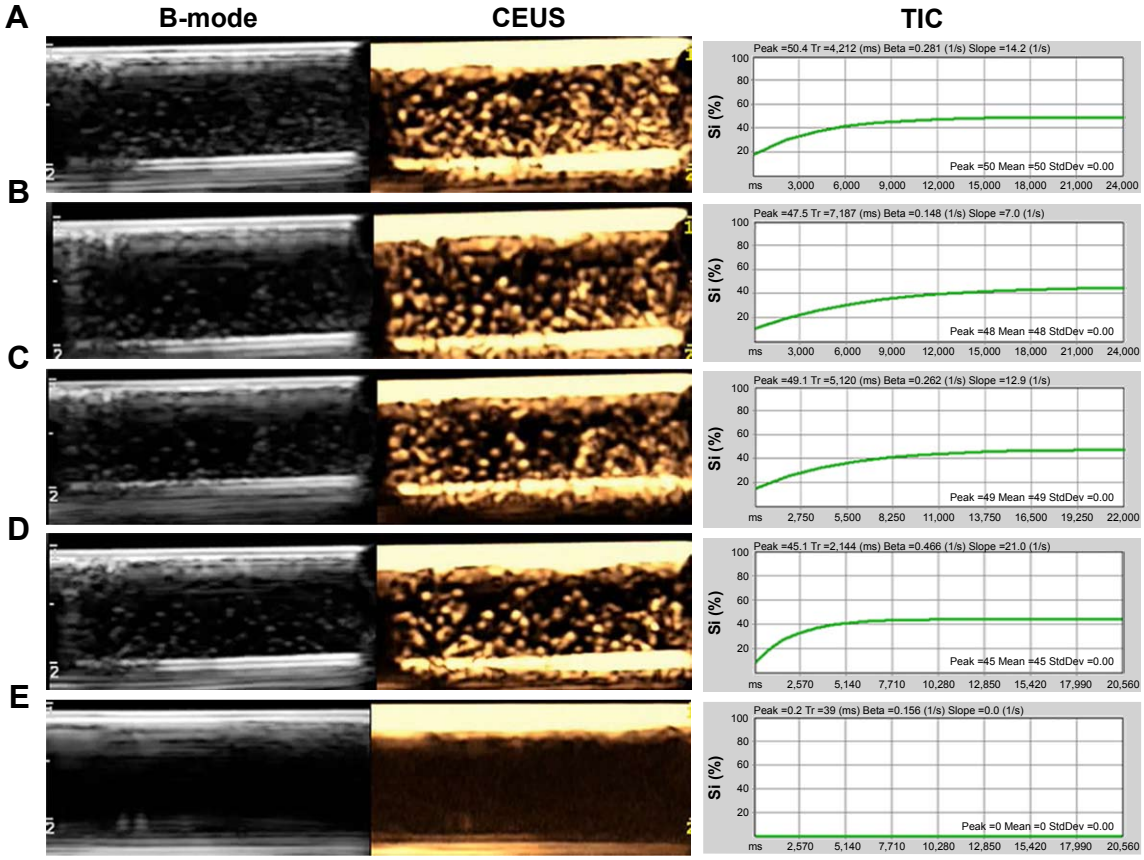

Figure 6 In vitro B-mode, CEUS images and TIC of (**A**) DNCs, (**B**) VNCs, (**C**) PNCs, (**D**) NNCs, and (**E**) pure degassed deionized water under the same concentration (0.5 mg/mL).

Notes: DNCs, dual-targeted gold nanoshelled poly(lactic-co-glycolic acid) nanocapsules carrying anti-vascular endothelial growth factor receptor type 2 antibody and anti-p53 antibody; NNCs, non-targeted gold nanoshelled poly(lactic-co-glycolic acid) nanocapsules; PNCs, single-targeted gold nanoshelled poly(lactic-co-glycolic acid) nanocapsules carrying anti-p53 antibody; TIC, time-intensity curves; VNCs, single-targeted gold nanoshelled poly(lactic-co-glycolic acid) nanocapsules carrying anti-vascular endothelial growth factor receptor type 2 antibody.

Abbreviations: B-mode, brightness mode; CEUS, contrast-enhanced ultrasound.

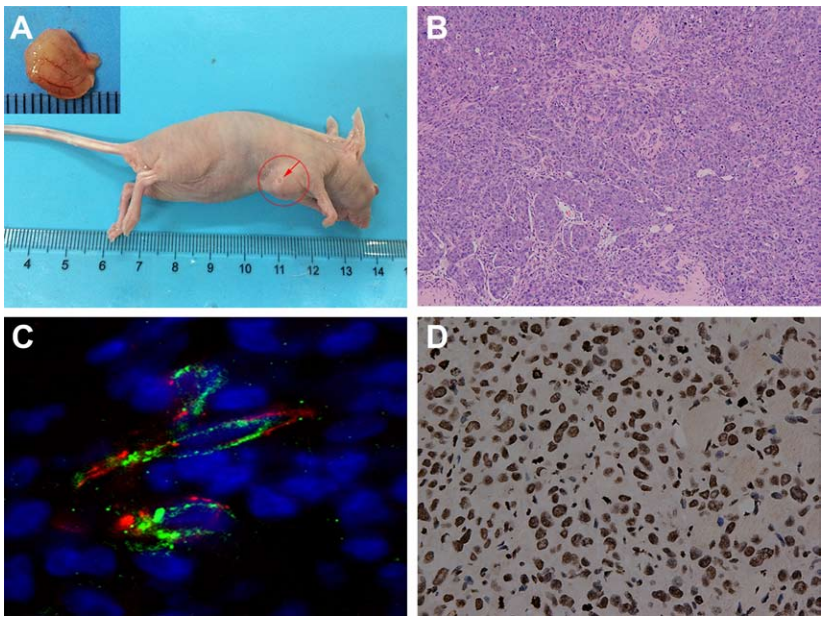

Figure 7 (**A**) MCF-7 orthotopic breast tumor nude mice model; (**B**) the H&E staining of tumor tissue (magnification: ×100); (**C**) merged confocal microscopic images of MCF-7 orthotopic breast tumor tissue after immunofluorescence staining of VEGFR2 (green), which overlap well with CD31-staining of vascular endothelial cells (red); (**D**) the IHC images of p53 protein (brown granules; magnification: ×400).

Abbreviations: CD-31, cluster of differentiation 31; IHC, immunohistochemistry; VEGFR2, vascular endothelial growth factor receptor type 2.

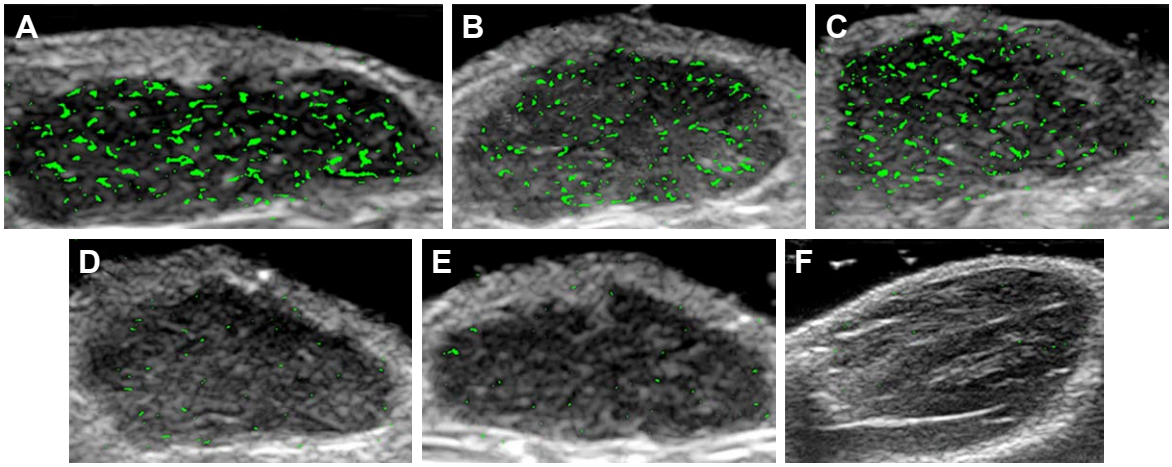

Figure 8 Transverse color-coded US images with (**A**) DNCs, (**B**) VNCs, (**C**) PNCs, (**D**)CNCs, (**E**) NNCs and in (**F**) the hind limb adductor muscle of mice using 22-MHz probe of MCF-7 orthotopic tumor from nude mice.

Notes: CNCs, free antibodies pre-treated before DNCs application; DNCs, dual-targeted gold nanoshelled poly(lactic-co-glycolic acid) nanocapsules carrying anti-vascular endothelial growth factor receptor type 2 antibody and anti-p53 antibody; NNCs, non-targeted gold nanoshelled poly(lactic-co-glycolic acid) nanocapsules; PNCs, single-targeted gold nanoshelled poly(lactic-co-glycolic acid) nanocapsules carrying anti-p53 antibody; VNCs, single-targeted gold nanoshelled poly(lactic-co-glycolic acid) nanocapsules carrying anti-vascular endothelial growth factor receptor type 2 antibody.

images in B-mode. The difference in video intensity from subtraction of pre- and post-destruction image frames was illustrated.[36] A dedicated small-animal US system with a 50-MHz probe recorded (digitally) dynamic images in contrast mode and overlaid the US-enhanced signal (green) on the background.[37]

As shown in Figure 8 and Table 2, differences in video intensity from subtraction of pre- and post-destruction images (green) on grayscale images were higher with DNCs (A) than with VNCs (B) or PNCs (C) ($P<0.05$). The intensity of the targeted competition group (D), which was pre-treated with free antibodies, was lower than that of the dual-targeted group ($P<0.001$). No obvious signal was detected in the hind-limb adductor muscle of mice (F) or after PLGA@Au NCs application (E). These results suggested that the targeting capability of DNCs was receptor-mediated through a combination of DNCs with p53 receptors on MCF-7 tumor cells and VEGFR2 on the endothelial cells of tumor vessels.

Table 2 Comparison of video intensity from subtraction in different experimental groups

Groups	Intensity (dB)
DNCs	146.15±4.37*‡§
VNCs	113.54±6.89‡§
PNCs	102.09±3.65‡§
CNCs	75.14±4.15
NNCs	61.25±3.12

Notes: *Significantly different from VNCs and PNCs ($P<0.05$). ‡Significantly differentfrom CNCs ($P<0.001$). §Significantly different from NNCs ($P<0.001$). Data are presented as means ± SD. CNCs, free antibodies pre-treated before DNCs application; DNCs, dual-targeted gold nanoshelled poly(lactic-co-glycolic acid) nanocapsules carrying anti-vascular endothelial growth factor receptor type 2 antibody and antip53 antibody; ICP-AES, inductively coupled plasma atomic emission spectroscopy; NNCs, non-targeted gold nanoshelled poly(lactic-co-glycolic acid) nanocapsules; PNCs, single-targeted gold nanoshelled poly(lactic-co-glycolic acid) nanocapsules carrying anti-p53 antibody; VNCs, single-targeted gold nanoshelled poly(lactic-coglycolic acid) nanocapsules carrying anti-vascular endothelial growth factor receptor type 2 antibody.

The results of the 50-MHz assay (Figure 9) were consistent with our observation using a 22-MHz probe. Compared with mice treated with non-targeted NCs, significant contrast enhancement at the tumor site was observed clearly after DNCs (A), VNCs (B), and PNCs (C) had been injected into the tail vein of mice, thereby indicating the high US efficiency of these NCs in vivo. Moreover, the intensity of DNCs was stronger than that for single-targeted NCs. The signal intensity in the tumor region was maintained at a steady level at the beginning, but the 3 targeted groups had increased signal intensity after 5 min, which could be ascribed to the binding of antibodies and receptors in vivo. In contrast to high US signal enhancement by DNCs, only weak intensity in the tumor was detected in the PLGA@Au NCs group (E) and mice when pretreated with free VEGFR2 and p53 antibodies (D) ($P<0.001$). These positive results of US in vivo suggested that DNCs could be used as a novel targeted US contrast agent for real-time monitoring of tumors.

Tumor immunohistochemistry

The merged CLSM image in Figure 7C showed that tumors stained positive for VEGFR2 (green), which compared well with the CD31 (red staining) of vascular endothelial cells. The immunohistochemical-staining image (Figure 7D) with

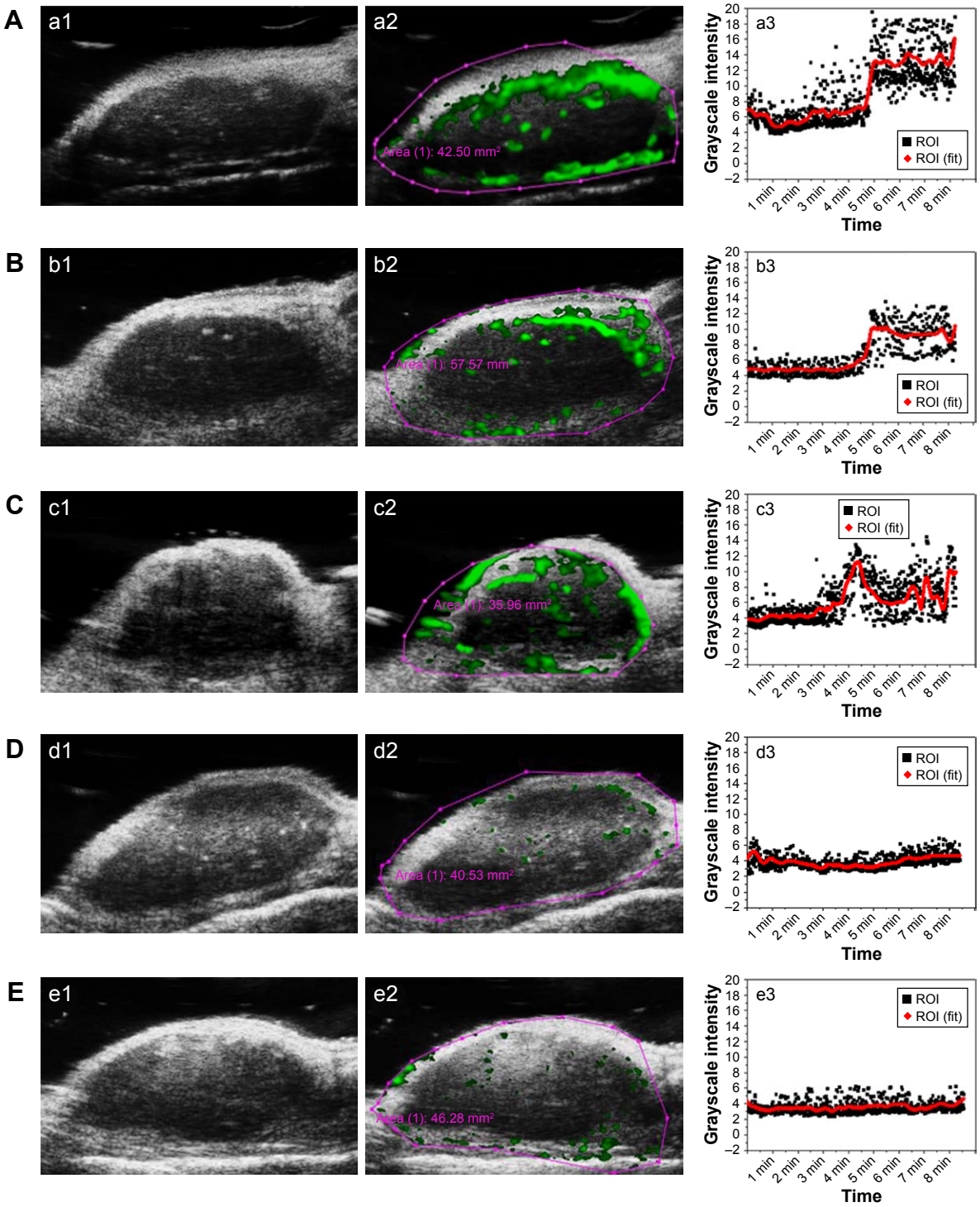

Figure 9 In vivo US imaging data using 50-MHz probe of MCF-7 orthotopic tumor from nude mice pre (a1–e1) and after (a2–e2) intravenous injection of DNCs (**A**), VNCs (**B**), PNCs (**C**), CNCs (**D**) and NNCs (**E**); (a3–e3) show the time-intensity curves.

Notes: CNCs, free antibodies pre-treated before DNCs application; DNCs, dual-targeted gold nanoshelled poly(lactic-co-glycolic acid) nanocapsules carrying anti-vascular endothelial growth factor receptor type 2 antibody and anti-p53 antibody; NNCs, non-targeted gold nanoshelled poly(lactic-co-glycolic acid) nanocapsules; PNCs, single-targeted gold nanoshelled poly(lactic-co-glycolic acid) nanocapsules carrying anti-p53 antibody; VNCs, single-targeted gold nanoshelled poly(lactic-co-glycolic acid) nanocapsules carrying anti-vascular endothelial growth factor receptor type 2 antibody; ROI (the region of interest), the red oval region in a2-e2.

brown granules was indicative of breast cancer tissues in MCF-7 mice expressing p53 protein. This finding suggested expression of VEGFR2 and p53 in breast tumors, providing pathologic evidence for targeted US in vivo.

Biodistribution of targeted NCs

High stability of targeted PLGA@Au NCs in blood is crucial for their further applications in vivo. This attractive feature also facilitated our in vivo biodistribution study.

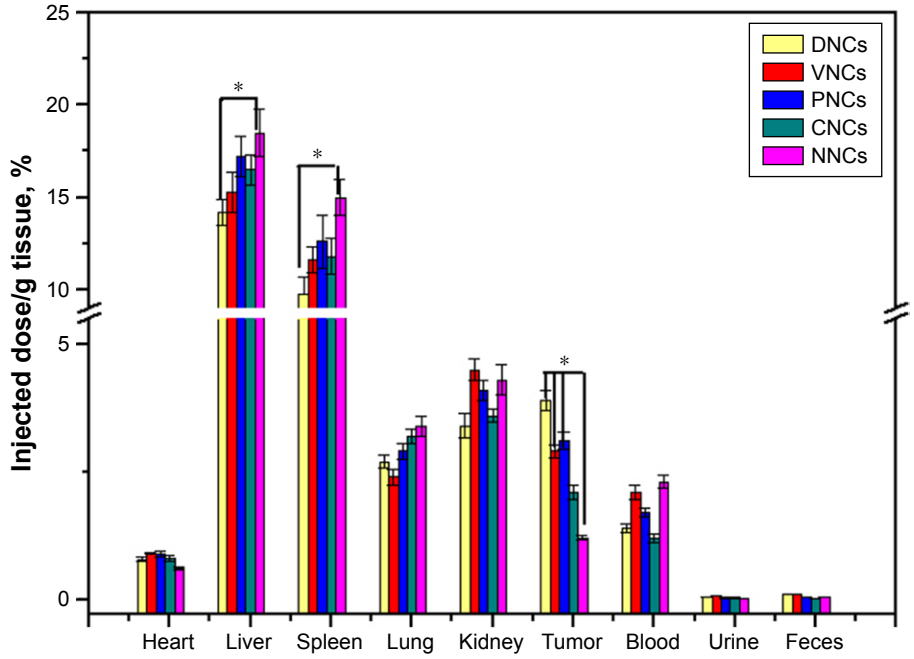

Figure 10 Biodistribution of Au determined by ICP-AES.
Notes: CNCs, free antibodies pre-treated before DNCs application; DNCs, dual-targeted gold nanoshelled poly(lactic-co-glycolic acid) nanocapsules carrying anti-vascular endothelial growth factor receptor type 2 antibody and anti-p53 antibody; NNCs, non-targeted gold nanoshelled poly(lactic-co-glycolic acid) nanocapsules; PNCs, single-targeted gold nanoshelled poly(lactic-co-glycolic acid) nanocapsules carrying anti-p53 antibody; VNCs, single-targeted gold nanoshelled poly(lactic-co-glycolic acid) nanocapsules carrying anti-vascular endothelial growth factor receptor type 2 antibody. *Significantly different from VNCs and NNCs.
Abbreviations: PLGA, poly(lactic-co-glycolic acid); ICP-AES, inductively coupled plasma atomic emission spectroscopy.

Mice were sacrificed after imaging and the amount of Au in major organs determined by ICP-AES. The biodistribution data (ID%/g) are presented in Figure 10. The liver was the dominant organ for accumulation of all types of PLGA@Au NCs, followed by the spleen, kidney, tumor, and lung. Heart, blood, urine, and feces showed relatively low Au concentrations. The ID%/g of DNCs in the liver and spleen was significantly lower than for non-targeted PLGA@Au NCs ($P<0.05$). Hence, dual-targeted NCs were "smarter" and could escape capture by liver or spleen cells compared with non-targeted NCs. No significant difference was found between dual- and single-targeted NCs. With regard to biodistribution in tumor tissues, more dual- and single-targeted PLGA@Au NCs accumulated in tumors than non-targeted NCs ($P<0.05$). DNCs had better targeting ability, but their concentration in tumor regions was lower than that in the liver and spleen. The actual in vivo pharmacokinetics of functional nanomaterials could be complicated. Hence, future efforts will focus on improving the biocompatibility and disguising ability of our DNCs in vivo for more satisfactory molecular imaging of early breast cancer. Furthermore, additional experiments will be conducted to assess the stability and functionality of DNCs. Also, a clinical-transformation study is needed to assess their effects over longer time periods.

Conclusion

DNCs, a novel molecular US agent that integrates targeted imaging of breast cancer cells with targeted imaging of tumor angiogenic vessels, was designed, fabricated, and evaluated in vitro and in vivo. Our results suggest that USMI using novel nano-sized, dual-targeted PLGA@Au NCs UCAs allows highly accurate and reliable detection of breast cancer in MCF-7 orthotopic mice. Our study lays the foundation for further development of promising tUCAs for early detection of breast cancer.

Acknowledgments

The present study was supported by the National Natural Science Foundation of China under Grant (number 81571678); the Natural Science Foundation of Shanghai under Grant (number 15ZR1425600); the Natural Science Foundation of Shanghai under Grant (number 14411968200); the Transverse Project of Renji Hospital, School of Medicine, Shanghai Jiao Tong University under Grant (number RJKY14-07); and Scientific Research and Cultivating Foundation of Renji Hospital affiliated to Shanghai Jiaotong University School of Medicine (No RJZZ17-015).

Disclosure

The authors report no conflicts of interest in this work.

References

1. Siegel RL, Miller KD, Jemal A. Cancer Statistics, 2017. *CA Cancer J Clin*. 2017;67(1):7–30.
2. Ghasemi M, Nabipour I, Omrani A, Alipour Z, Assadi M. Precision medicine and molecular imaging: new targeted approaches toward cancer therapeutic and diagnosis. *Am J Nucl Med Mol Imaging*. 2016; 6(6):310–327.
3. Chakravarty R, Chakraborty S, Dash A. Molecular imaging of breast cancer: role of RGD Peptides. *Mini Rev Med Chem*. 2015;15(13): 1073–1094.
4. Anderson CR, Hu X, Zhang H, et al. Ultrasound molecular imaging of tumor angiogenesis with an integrin targeted microbubble contrast agent. *Invest Radiol*. 2011;46(4):215–224.
5. Kiser J. Molecular imaging and its role in the management of breast cancer. *Clin Obstet Gynecol*. 2016;59(2):403–411.
6. Funke M. Diagnostic imaging of breast cancer: an update. *Radiologe*. 2016;56(10):921–938.
7. Abou-Elkacem L, Wilson KE, Johnson SM, et al. Ultrasound molecular imaging of the breast cancer neovasculature using engineered fibronectin scaffold ligands: a novel class of targeted contrast ultrasound agent. *Theranostics*. 2016;6(11):1740–1752.
8. Yang F, Chen ZY, Lin Y. Advancement of targeted ultrasound contrast agents and their applications in molecular imaging and targeted therapy. *Curr Pharm Design*. 2013;19(8):1516–1527.
9. Kiessling F, Bzyl J, Fokong S, Siepmann M, Schmitz G, Palmowski M. Targeted ultrasound imaging of cancer: an emerging technology on its way to clinics. *Curr Pharm Design*. 2012;18(15):2184–2199.
10. Perera RH, Hernandez C, Zhou H, Kota P, Burke A, Exner AA. Ultrasound imaging beyond the vasculature with new generation contrast agents. *Wiley Interdiscip Rev Nanomed Nanobiotechnol*. 2015;7(4): 593–608.
11. Lv J-M, Wang X, Marin-Muller C, et al. Current advances in research and clinical applications of PLGA based nanotechnology. *Expert Rev Mol Design*. 2009;9(4):325–341.
12. Nestor MM, Kei NP, Guadalupe NA, Elisa ME, Adriana GQ, David QG. Preparation and in vitro evaluation of poly(D,L-lactide-co-glycolide) air-filled nanocapsules as a contrast agent for ultrasound imaging. *Ultrasonics*. 2011;51(7):839–845.
13. Xia K, Zhang L, Huang Y, Lu Z. Preparation of gold nanorods and their applications in photothermal therapy. *J Nanosci Nanotechnol*. 2015; 15(1):63–73.
14. Kim D, Jeong YY, Jon S. A drug-loaded aptamer-gold nanoparticle bioconjugate for combined CT imaging and therapy of prostate cancer. *ACS Nano*. 2010;4(7):3689–3696.
15. Ke H, Wang J, Dai Z, et al. Gold-nanoshelled microcapsules: a theranostic agent for ultrasound contrast imaging and photothermal therapy. *Angew Chem Ind Ed Engl*. 2011;50(13):3017–3021.
16. Ke H, Wang J, Tong S, et al. Gold nanoshelled liquid perfluorocarbon magnetic nanocapsules: a nanotheranostic platform for bimodal ultrasound/magnetic resonance imaging guided photothermal tumor ablation. *Theranostics*. 2013;4(1):12–23.
17. Ke H, Yue X, Wang J, et al. Gold nanoshelled liquid perfluorocarbon nanocapsules for combined dual modal ultrasound/CT imaging and photothermal therapy of cancer. *Small*. 2014;10(6):1220–1227.
18. Xi J, Qian X, Qian K, et al. Au nanoparticle-coated, PLGA-based hybrid capsules for combined ultrasound imaging and HIFU therapy. *J Mater Chem B*. 2015;3(20):4213–4220.
19. Hutchinson L. Breast cancer: challenges, controversies, breakthroughs. *Nat Rev Clin Oncol*. 2010;7(12):669–670.
20. Behdani M, Zeinali S, Karimipour M, et al. Development of VEGFR2-specific Nanobody Pseudomonas exotoxin A conjugated to provide efficient inhibition of tumor cell growth. *N Biotechnol*. 2013;30(2): 205–209.
21. Martinez JO, Evangelopoulos M, Karun V, et al. The effect of multistage nanovector targeting of VEGFR2 positive tumor endothelia on cell adhesion and local payload accumulation. *Biomaterials*. 2014; 35(37):9824–9832.
22. Chinnasamy D, Tran E, Yu Z, Morgan RA, Restifo NP, Rosenberg SA. Simultaneous targeting of tumor antigens and the tumor vasculature using T lymphocyte transfer synergize to induce regression of established tumors in mice. *Cancer Res*. 2013;73(11):3371–3380.
23. Warram JM, Sorace AG, Saini R, Umphrey HR, Zinn KR, Hoyt K. A triple-targeted ultrasound contrast agent provides improved localization to tumor vasculature. *J Ultrasound Med*. 2011;30(7):921–931.
24. Pochon S, Tardy I, Bussat P, et al. BR55: a lipopeptide-based VEGFR2-targeted ultrasound contrast agent for molecular imaging of angiogenesis. *Invest Radiol*. 2010;45(2):89–95.
25. Bzyl J, Lederle W, Palmowski M, Kiessling F. Molecular and functional ultrasound imaging of breast tumors. *Eur J Radiol*. 2012;81(Suppl 1): S11–S12.
26. Bachawal SV, Jensen KC, Lutz AM, et al. Earlier detection of breast cancer with ultrasound molecular imaging in a transgenic mouse model. *Cancer Res*. 2013;73(6):1689–1698.
27. Lee DS, Kim SH, Suh YJ, Kim S, Kim HK, Shim BY. Clinical implication of p53 overexpression in breast cancer patients younger than 50 years with a triple-negative subtype who undergo a modified radical mastectomy. *Jpn J Clin Oncol*. 2011;41(7):854–866.
28. Sana M, Malik HJ. Current and emerging breast cancer biomarkers. *J Cancer Res Ther*. 2015;11(3):508–513.
29. Milicevic Z, Bajic V, Zivkovic L, Kasapovic J, Andjelkovic U, Spremo-Potparevic B. Identification of p53 and its isoforms in human breast carcinoma cells. *TheScientificWorldJournal*. 2014;2014:1–10.
30. Xu L, Wan C, Du J, et al. Synthesis, characterization, and in vitro evaluation of targeted gold nanoshelled poly(d,l-lactide-co-glycolide) nanoparticles carrying anti p53 antibody as a theranostic agent for ultrasound contrast imaging and photothermal therapy. *J Biomater Sci Polym Ed*. 2017;28(4):415–430.
31. Wang C-W, Yang S-P, Hu H, Du J, Li F-H. Synthesis, characterization and in vitro and in vivo investigation of C3F8-filled poly(lactic-co-glycolic acid) nanoparticles as an ultrasound contrast agent. *Mol Med Rep*. 2015;11(3):1885–1890.
32. Zhang XD, Luo Z, Chen J, et al. Storage of gold nanoclusters in muscle leads to their biphasic in vivo clearance. *Small*. 2015;11(14): 1683–1690.
33. Liu J, Li J, Rosol TJ, Pan X, Voorhees JL. Biodegradable nanoparticles for targeted ultrasound imaging of breast cancer cells in vitro. *Phys Med Biol*. 2007;52(16):4739–4747.
34. Yang H, Cai W, Xu L, et al. Nanobubble-Affibody: novel ultrasound contrast agents for targeted molecular ultrasound imaging of tumor. *Biomaterials*. 2015;37:279–288.
35. Kohl Y, Kaiser C, Bost W, et al. Preparation and biological evaluation of multifunctional PLGA-nanoparticles designed for photoacoustic imaging. *Nanomedicine*. 2011;7:228–237.
36. Willmann JK, Paulmurugan R, Chen K, et al. US imaging of tumor angiogenesis with microbubbles targeted to vascular endothelial growth factor receptor type 2 in mice. *Radiology*. 2008;246(2):508–518.
37. Wu H, Shi H, Zhang H, et al. Prostate stem cell antigen antibody-conjugated multiwalled carbon nanotubes for targeted ultrasound imaging and drug delivery. *Biomaterials*. 2014;35(20):5369–5380.

International Journal of Nanomedicine

Dovepress

Publish your work in this journal

The International Journal of Nanomedicine is an international, peer-reviewed journal focusing on the application of nanotechnology in diagnostics, therapeutics, and drug delivery systems throughout the biomedical field. This journal is indexed on PubMed Central, MedLine, CAS, SciSearch®, Current Contents®/Clinical Medicine, Journal Citation Reports/Science Edition, EMBase, Scopus and the Elsevier Bibliographic databases. The manuscript management system is completely online and includes a very quick and fair peer-review system, which is all easy to use. Visit http://www.dovepress.com/testimonials.php to read real quotes from published authors.

Submit your manuscript here: http://www.dovepress.com/international-journal-of-nanomedicine-journal